Impedance-Based Stability Analysis for Interconnected Converter Systems With Open-Loop RHP Poles

Yicheng Liao, *Student Member, IEEE*, and Xiongfei Wang, *Senior Member, IEEE*

***Abstract*—The small-signal stability of interconnected converter systems can be tackled by the impedance-based analysis method, where the Bode plots of the individual impedances derived from subsystems are utilized for a design-oriented analysis. However, those methods only apply to the interconnected systems without having open-loop right-half-plane (RHP) poles. This article thus proposes a general stability analysis method based on Bode plots of individual impedances, which allows considering the open-loop RHP poles and shaping the impedances for stabilizing the system. Experimental case studies on the current control interactions of two paralleled grid-tied inverters validate the effectiveness of the method.**

***Index Terms*—Bode plots, impedance-based analysis, interconnected converters, right-half-plane (RHP) poles, stability.**

I. Introduction

In RECENT years, the increasing use of power electronic converters has brought more stability issues to modern power systems, such as the sideband oscillations of the fundamental frequency and harmonic oscillations [1]. The impedance-based analysis provides an attractive approach for addressing the small-signal stability of interconnected converter systems. The general idea is to divide the system into two subsystems at a given point of common coupling (PCC), and then the ratio of the impedances of subsystems can serve as the open-loop gain of the whole system, through which the system dynamics can be assessed based on the Nyquist stability criterion (NSC). In this method, only the terminal impedances of subsystems are required, which can be obtained by the frequency scanning, and thus facilitates the stability assessment for the "black-box" systems whose internal parameters are unknown.

The extensive applications of the impedance-based method date back to 1976 by Undrill and Kostyniak, where the subsynchronous oscillations of power systems are analyzed based on the impedances of generators and the transmission network [2]. In the same year, Middlebrook first applied the method to design the input filters of dc–dc power converters [3], where the system stability is guaranteed by confining the minor loop gain, which is defined as the ratio of the filter impedance and the converter input impedance, within the unity circle on the complex plane.

Later on, the minor loop gain was defined as the source-load impedance ratio for distributed power systems (DPSs), and by preventing the minor loop gain from entering the so-called forbidden regions. Wildrick *et al*. developed a method for the impedance specification with the aid of Bode plots for a stable DPS, also known as the gain margin and phase margin criterion [4]. This work is followed by some more impedance specification methods developed for DPSs, where different forbidden regions were introduced [5]–[8]. In contrast to the Nyquist diagram of the impedance ratio, a prominent feature of utilizing the Bode plots of individual impedances is that the interactions between impedances can be revealed graphically, and the impedances of subsystems can be shaped to meet the predefined stability margin [9]–[11]. However, all those methods assume that no right-half-plane (RHP) poles exist in the impedance ratio [12]. This precondition can be readily met in $Z + Y$ systems [13]–[17], where the impedance ratio is Z/Y, and both subsystems are internally stable, i.e., Z and Y have no RHP poles.

Besides $Z + Y$ systems, there are also $Z + Z$ or $Y + Y$ systems in the paralleled converter systems [18]–[21], where the RHP poles may exist in the impedance ratio, i.e., Z/Z or Y/Y, due to the presence of RHP zeros in Z or Y. Consequently, the prior knowledge on the number of open-loop RHP poles is required according to the NSC [22], [23]. To avoid introducing the open-loop RHP poles in the impedance-based analysis, an impedance/admittance sum criterion was developed recently [18]. Instead of deriving the impedance ratio, the impedance sum is used in this method to calculate the whole system's closed-loop characteristic polynomial (CLCP), which can then be analyzed based on Cauchy's Argument Principle. Alternatively, the multiloop NSC [24] was also employed for analyzing the paralleled converter systems with open-loop RHP poles [21]. However, all these approaches regard the impedance ratio or the impedance sum as a whole, and hence the impedances of subsystems cannot be explicitly specified and shaped as the case without open-loop RHP poles in [4].

This article proposes a general approach to the impedance-based stability analysis of interconnected converter systems, which allows using the Bode plots of individual impedances even if there are RHP poles in the minor loop gain.

Manuscript received January 16, 2019; revised April 10, 2019 and May 18, 2019; accepted September 2, 2019. Date of publication September 5, 2019; date of current version January 10, 2020. Recommended for publication by Associate Editor F. H. Khan. *(Corresponding author: Xiongfei Wang.)*

The authors are with the Department of Energy Technology, Aalborg University, Aalborg 9220, Denmark (e-mail: ycl@et.aau.dk; xwa@et.aau.dk).

Color versions of one or more of the figures in this article are available online at http://ieeexplore.ieee.org.

Digital Object Identifier 10.1109/TPEL.2019.2939636

TABLE I
COMPARISON OF DIFFERENT IMPEDANCE-BASED STABILITY ANALYSIS METHODS

Method	NSC	Impedance specification (forbidden regions)	Impedance sum criterion	Multi-loop NSC
Theoretical bases	Impedance ratio (minor loop gain)	Individual impedances (minor loop gain)	Impedance sum (CLCP)	Multiple impedance ratios (multiple minor loop gains)
Constraints	Not available for individual impedance shaping	Assuming that no open-loop RHP poles exist in the impedance ratio (Z+Y)	Assuming that no RHP poles in the impedance sum (Z+Z)	Check the system topology for selecting multiple loops
References	[2], [15], [23], [26]	[3]–[8]	[18], [19], [20], [29]	[21]

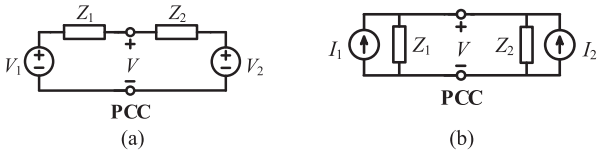

Fig. 1. General interconnected system. (a) Thevenin's equivalence. (b) Norton's equivalence.

Thus, the impedances of subsystems can be readily specified and shaped for stabilizing the whole system. The rest of this article is organized as follows: Section II presents a comparison of the existing impedance-based stability analysis methods with respect to their theoretical bases and constraints. Section III proposes the general method for the impedance-based stability analysis. Section IV provides the experimental results to validate the effectiveness of the method. Finally, conclusions are drawn in Section V, where the advantages of the proposed method are summarized.

II. EXISTING IMPEDANCE-BASED STABILITY ANALYSIS METHODS

In this section, a critical review of the existing impedance-based stability analysis methods is given, through which their constraints are summarized.

A. System Modeling

An interconnected converter system can be modeled as two subsystems connected at the PCC. Each subsystem can be represented by a voltage source in series with an impedance or a current source in parallel with an impedance, according to the Thevenin's theorem or the Norton's theorem, as shown in Fig. 1. Then the voltages at the PCCs in Fig. 1(a) and (b) can be, respectively, expressed as

$$V = \frac{Z_2}{Z_1+Z_2}V_1 + \frac{Z_1}{Z_1+Z_2}V_2 = \frac{1}{1+\frac{Z_1}{Z_2}}V_1 + \frac{\frac{Z_1}{Z_2}}{1+\frac{Z_1}{Z_2}}V_2 = \frac{\frac{Z_2}{Z_1}}{1+\frac{Z_2}{Z_1}}V_1 + \frac{1}{1+\frac{Z_2}{Z_1}}V_2 \quad (1)$$

$$V = \frac{Z_1Z_2}{Z_1+Z_2}I_1 + \frac{Z_1Z_2}{Z_1+Z_2}I_2 = \frac{Z_1}{1+\frac{Z_1}{Z_2}}I_1 + \frac{Z_1}{1+\frac{Z_1}{Z_2}}I_2 = \frac{Z_2}{1+\frac{Z_2}{Z_1}}I_1 + \frac{Z_2}{1+\frac{Z_2}{Z_1}}I_2. \quad (2)$$

Equations (1) and (2) are both established in the s domain with "s" omitted for brevity. It can be seen that $Z_1 + Z_2$ serves as the denominator of the closed-loop transfer function, while the impedance ratios Z_1/Z_2 or Z_2/Z_1 represents the open-loop gain. Consequently, the stability of the interconnected system relies on the terminal impedances of the two subsystems.

B. Comparison of the Existing Methods

Table I provides a comparison of the existing impedance-based stability analysis methods with respect to their theoretical bases and constraints. These methods are categorized into four classes: NSC, impedance specification methods, impedance sum criterion, and multiloop NSC.

The first two categories of the approaches analyze the system stability through the minor loop gain, i.e., the impedance ratio of the interconnected system. The NSC analyzes the impedance ratio directly by Nyquist diagrams, which thus requires prior knowledge of the number of open-loop RHP poles. To do that, the parametric model of the impedance ratio, which can be obtained by either the analytical derivation [26] or the transfer-function fitting [28], is generally employed. Compared with the NSC, the distinguished feature of the impedance specification methods is that the individual impedances of subsystems can be directly evaluated on Bode plots, instead of analyzing their ratio with Nyquist diagrams. Yet, a prerequisite for doing that is no RHP poles exist in the impedance ratio, which thus limits those impedance specification methods to $Z + Y$ systems.

Instead of the minor loop gain based on the impedance ratio, the impedance sum is used for the stability analysis in the third method. From (1) and (2), it can be found that the impedance sum forms the denominator of the closed-loop transfer function [18], [29], and thus the number of RHP zeros in the impedance sum determines the system stability, which can be readily checked by the encirclement of origin in the complex plane. However, this method only applies to $Z + Z$ or $Y + Y$ systems, where there are no RHP poles in Z or Y.

Differing from the impedance ratio given in (1) and (2), the multiloop NSC [30] formulates the interconnected system shown in Fig. 1 into a multiloop feedback system, where the subsystems can be seen as multiple feedback loops, which are closed sequentially, and then a series of Nyquist diagrams for the open-loop gain of each loop can be drawn for the stability analysis [21]. Thus, the issues of introducing open-loop RHP

poles can be avoided. Yet, a full knowledge of the system topology is needed for selecting multiple feedback loops.

Therefore, only the second method, among other alternative schemes, allows specifying the impedance in Bode plots, yet it merely applies to the $Z + Y$ systems, which have no open-loop RHP poles. The other three categories of approaches are based on either the impedance ratio or the impedance sum, where the effect of individual impedance cannot be intuitively modeled.

III. General Method of Impedance-Based Stability Analysis

In this section, a general method for the stability analysis of interconnected converter systems is introduced. The method is derived from the NSC applied to the minor loop gain, yet is formulated on Bode plots of individual impedances, which allows shaping the impedances of subsystems to stabilize the entire system, even for cases with open-loop RHP poles.

Similar to the existing methods based on minor loop gains, the proposed method also consists of four general stages: the formulation of the minor loop gain; the identification of open-loop RHP poles; the identification of crossings; the stability prediction and the impedance specification.

A. Formulation of the Minor Loop Gain

First, a method of defining the impedance ratio is presented, which does not rely on the subsystem types (Type *Z* or Type *Y* [19]). Therefore, it is applicable in the stability analysis for "black-box" systems.

It is noted that the NSC assumes that the open-loop transfer function is a proper function [25], which implies that the order of the numerator is lower than that of the denominator, or the frequency response of the transfer function approaches to zero (corresponding to the origin on the Nyquist plot) at the infinite frequency [27]. Thus, the part of the Nyquist plot when *s* traverses along the infinite semicircle on the right-half complex plane can be ignored. However, for an artificially defined impedance ratio, this condition may not hold. If the impedance ratio is improper, the NSC cannot be readily used for the stability analysis, due to the nonzero value of the frequency response at the infinite frequency. Then the inverse NSC is a better choice [22], [23]. Hence, it is suggested to define the impedance ratio as a proper transfer function, which is named as the proper impedance ratio and satisfies that

$$\lim_{\omega\to\infty}\frac{Z_1(j\omega)}{Z_2(j\omega)}=0. \tag{3}$$

The above equation implies that the proper impedance ratio is formulated as the minor loop gain, since $|Z_1| < |Z_2|$ at the infinite frequency. In the cases of designing input filters for dc–dc converters [3], the source-load interactions in DPSs [4]–[8], the load-source interactions in current-source converter systems [14], [15], and the $Z + Y$ systems [16], the impedance ratios are all formulated as proper impedance ratios.

It is worth noting that in a practical system the frequency response at the infinite frequency may be unknown. Then, the formulation of the impedance ratio can be determined by the available high-frequency responses and their derivatives of the impedance magnitudes. More specifically, the minor loop gain can be defined in the following way.

1) If the two impedances have the different magnitude slopes at higher frequencies, the impedance with the smaller magnitude slope should be chosen as the numerator of the minor loop gain. Then the other impedance is chosen as the denominator of the minor loop gain.
2) If the two impedances have the same magnitude slope at higher frequencies, the impedance with the smaller magnitude should be chosen as the numerator of the minor loop gain. Then the other impedance is chosen as the denominator of the minor loop gain.

B. Identification of Open-Loop RHP Poles

As the impedance ratio is intentionally defined as a proper function regardless of the subsystem types, the open-loop RHP poles may be introduced, leading to a nonminimum-phase minor loop gain [27]. Hence, the number of open-loop RHP poles has to be checked prior to the stability analysis.

Considering that the subsystem types are often unknown in practice, the impedances may have RHP poles or RHP zeros, e.g., the RHP zeros may be present in the output impedance of a Type-Z system, while the RHP poles may be present in the output impedance of a Type-Y system. Then the number of open-loop RHP poles is calculated as

$$\mathcal{P}[Z_1/Z_2]=\mathcal{P}[Z_1]+\mathcal{Z}[Z_2] \tag{4}$$

where $\mathcal{P}$ denotes the number of RHP poles, and $\mathcal{Z}$ denotes the number of RHP zeros.

There are several ways to identify the number of RHP poles and RHP zeros. One commonly used method is to do parametric identifications of the measured impedance [28], and then plot the pole-zero map of the fitted impedance transfer function. Alternatively, a frequency-response-based method of checking zero-crossing points on the real and imaginary axes in the complex plane of the transfer function is discussed in [29]. In this article, a simple approach to identifying the RHP poles and zeros directly from the impedance Bode plot is adopted. For nonminimum-phase systems, an RHP pole can result in the magnitude slope change of -20 dB/dec and the phase change of $+90°$, whereas an RHP zero can lead to the magnitude slope change of $+20$ dB/dec and the phase change of $-90°$ [27]. According to the magnitude slope change and the phase change, the number of RHP poles and zeros can be determined based on Bode plots even if there are close left-half-plane (LHP) zeros and LHP poles, provided that RHP poles and RHP zeros do not coexist. The specific identification procedure is illustrated as follows:

$$Z_{\mathrm{RHP}}+Z_{\mathrm{LHP}}-P_{\mathrm{RHP}}-P_{\mathrm{LHP}}=\frac{(\mathrm{d}|Z|/\mathrm{d}f)_{\mathrm{high}-f}-(\mathrm{d}|Z|/\mathrm{d}f)_{\mathrm{low}-f}}{20\ \mathrm{dB/dec}} \tag{5}$$

$$-Z_{\mathrm{RHP}}+Z_{\mathrm{LHP}}+P_{\mathrm{RHP}}-P_{\mathrm{LHP}}=\frac{\angle Z_{\mathrm{high}-f}-\angle Z_{\mathrm{low}-f}}{90^\circ} \tag{6}$$

$$Z_{\mathrm{RHP}}=0\,\mathrm{or}\,P_{\mathrm{RHP}}=0 \tag{7}$$

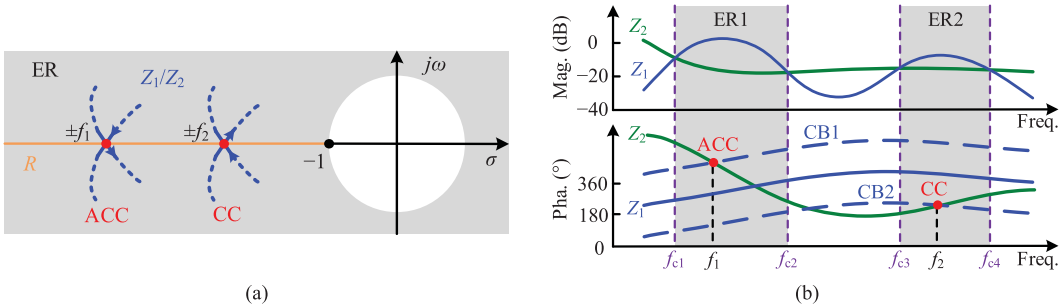

Fig. 2. Illustration of the number of encirclements around the critical point. (a) Nyquist plot. (b) Bode plot.

where Z_{RHP}, Z_{LHP}, P_{RHP}, and P_{LHP} denote the numbers of zeros and poles on the corresponding half planes. $\mathrm{d}|Z|/\mathrm{d}f$ represents the impedance magnitude slope at high frequencies or low frequencies, and $\angle Z$ denotes the impedance phase. $Z_{\mathrm{RHP}}-P_{\mathrm{RHP}}$ can be obtained by subtracting (6) from (5), and then depending on the sign ($\pm$) of $Z_{\mathrm{RHP}}-P_{\mathrm{RHP}}$ and considering (7), both Z_{RHP} and P_{RHP} can be determined.

However, it is worth noting that this identification method does not theoretically apply when several close RHP poles and RHP zeros coexist. The same challenge is also posed to the parametric identification method [28]. Hence, it is important to avoid introducing several close RHP poles and RHP zeros when partitioning a complex converter-based power system. This is because the presence of RHP poles and RHP zeros is highly dependent on how to aggregate the impedances of subsystems [29]. There will be no RHP poles and RHP zeros coexisting if the system can be properly partitioned based on the properties of subsystems (Type Z or Type Y) [7].

C. Identification of Crossings

If $\mathcal{N}$ denotes the total number of clockwise encirclements around the critical point $(-1, j0)$ on the Nyquist plot, according to the NSC, the system is stable if and only if

$$\mathcal{N}\left[Z_1/Z_2\right] = -\mathcal{P}\left[Z_1/Z_2\right] \tag{8}$$

where $\mathcal{P}\left[Z_1/Z_2\right]$ can be obtained by (4) on the Bode plots of Z_1 and Z_2. Then, a graphical method of determining $\mathcal{N}\left[Z_1/Z_2\right]$ by using the Bode plots of individual impedances is introduced in the rest of this section. The method transfers the minor-loop-gain analysis on the Nyquist diagram to the individual-impedance analysis on the Bode plot.

Fig. 2 maps the encirclements around the critical point from the Nyquist plot to the Bode plot. It is noted that the mapping relationship is not as simple as the case without the open-loop RHP poles, since the phase derivative term on Bode plots is involved in determining the encirclement types [31], [32], which is, however, overlooked by the existing impedance-specification methods [3]–[8]. The detailed mapping process is introduced as follows:

1) Crossings on the Nyquist Plot: The number of encirclements around the critical point $(-1, j0)$ can be determined by the number of crossings over $(-\infty, -1)$ on the real axis in the Nyquist plot of Z_1/Z_2 [33], [34], as denoted by R in Fig. 2(a). It can be seen that R locates in the exterior region (ER) of the unity circle, as denoted by the shaded area. There may be two types of crossings in the ER, i.e., one is the clockwise crossing (CC), and the other is the anticlockwise crossing (ACC). Thus the total number of crossings can be formulated as

$$\mathcal{N}\left[Z_1/Z_2\right] = \mathcal{N}_{\mathrm{CC}}\left[Z_1/Z_2\right] - \mathcal{N}_{\mathrm{ACC}}\left[Z_1/Z_2\right] \tag{9}$$

where both $\mathcal{N}_{\mathrm{CC}}\left[Z_1/Z_2\right]$ and $\mathcal{N}_{\mathrm{ACC}}\left[Z_1/Z_2\right]$ are nonnegative integers. They can be obtained by (10) and (11)

$$\begin{aligned}\mathcal{N}_{\mathrm{CC}}\left[Z_1/Z_2\right] = \Bigg|\Bigg\{\omega\in\mathbb{R}\Big|\left|\frac{Z_1}{Z_2}(j\omega)\right|>1 \text{ and } \angle\frac{Z_1}{Z_2}(j\omega)\\ = \pm 180^\circ \text{ and } \frac{d}{d\omega}\frac{Z_1}{Z_2}(j\omega)<0\Bigg\}\Bigg|\end{aligned} \tag{10}$$

$$\begin{aligned}\mathcal{N}_{\mathrm{ACC}}\left[Z_1/Z_2\right] = \Bigg|\Bigg\{\omega\in\mathbb{R}\Big|\left|\frac{Z_1}{Z_2}(j\omega)\right|>1 \text{ and } \angle\frac{Z_1}{Z_2}(j\omega)\\ = \pm 180^\circ \text{ and } \frac{d}{d\omega}\frac{Z_1}{Z_2}(j\omega)>0\Bigg\}\Bigg|.\end{aligned} \tag{11}$$

It is noted from (10) and (11) that the direction of the Nyquist diagram is related to the derivative of the phase response of Z_1/Z_2 versus the frequency. Within the ER, a crossing over $\pm 180^\circ$ with a positive derivative indicates an ACC, and a crossing over $\pm 180^\circ$ with a negative derivative indicates a CC.

2) Crossings on Impedance Bode Plots: The generalized Bode criterion (GBC) [35], [36] provides a rigorous method to directly determine the crossings over R on the Nyquist diagram using Bode plots. According to the GBC, the total number of crossings can be determined by the Bode plot of the loop gain, as well as the 0 Hz frequency responses. The Bode plot does illustrate the crossings for all the nonzero frequencies, yet the crossings at 0 Hz still needs to be counted separately. It is assumed that there are one ACC at f_1 and one CC at f_2 ($f_1 \neq 0$ and $f_2 \neq 0$), as seen from Fig. 2(a). From the Nyquist plot, the crossing type at $-f_1$ should be the same as that at f_1, and similarly for the crossing type at $\pm f_2$. Therefore, for $f \neq 0$, the total crossing number can be determined as two times the number of phase crossings over $(2k+1)180^\circ$ in the ER where the magnitude is larger than 0 dB on Bode plots. While for $f =$ 0 Hz, the number of crossings should only be counted once.

TABLE II
IDENTIFICATION RULE OF THE NUMBER OF ENCIRCLEMENTS ON BODE PLOTS

Steps		Mathematical representation
Step 1	Find all the ERs, as denoted by the shaded areas.	$\lvert Z_1(j\omega)\rvert > \lvert Z_2(j\omega)\rvert$
Step 2	Check whether there are crossings within the ERs with the aid of CBs, as denoted by the red dots.	$\angle Z_1(j\omega) - \angle Z_2(j\omega) = \pm 180^\circ$
Step 3	Determine the crossing types if the crossings exist.	$\frac{\mathrm{d}}{\mathrm{d}\omega}\angle Z_1(j\omega) < \frac{\mathrm{d}}{\mathrm{d}\omega}\angle Z_2(j\omega)$ for a CC $\frac{\mathrm{d}}{\mathrm{d}\omega}\angle Z_1(j\omega) > \frac{\mathrm{d}}{\mathrm{d}\omega}\angle Z_2(j\omega)$ for an ACC
Step 4	Calculate the number of crossings.	$\mathcal{N}_{\mathrm{CC}}[Z_1/Z_2] = 2n_{\mathrm{cc}} + n_{\mathrm{cc0}}$ [a] $\mathcal{N}_{\mathrm{ACC}}[Z_1/Z_2] = 2n_{\mathrm{acc}} + n_{\mathrm{acc0}}$ [b] $\mathcal{N}[Z_1/Z_2] = \mathcal{N}_{\mathrm{CC}}[Z_1/Z_2] - \mathcal{N}_{\mathrm{ACC}}[Z_1/Z_2]$

Notes: $\mathcal{N}$—number of crossings on the Nyquist plot; n—number of crossings on the Bode plot.
a. n_{cc}—number of CCs for $\omega \neq 0$, n_{cc0}—number of CCs at $\omega = 0$;
b. n_{acc}—number of ACCs for $\omega \neq 0$, n_{acc0}—number of ACCs at $\omega = 0$.

Then based on (10) and (11) by separating Z_1 and Z_2 with the superposition principle, the rules for directly identifying the number of encirclements based on the individual impedances are proposed in Table II, which consists of four steps.

Fig. 2(b) gives a schematic representation of the impedance Bode plots of Z_1 and Z_2, where an ACC at f_1 and a CC at f_2 within the ER correspond to the Nyquist plot shown in Fig. 2(a). Each step of the proposed rules is introduced as follows:

1) *Step 1:* The ERs outside the unity circle of the Nyquist diagram are found as all the frequency intervals where the numerator impedance (Z_1) is larger than the denominator impedance (Z_2), as denoted by the shaded areas in Fig. 2.
2) *Step 2:* Two auxiliary boundaries are defined by shifting one impedance-phase curve (i.e., $\angle Z_1$) of $\pm 180^\circ$ in order to help identify the number of crossings, which are denoted as two crossing boundaries (CBs). If the other impedance-phase curve (i.e., $\angle Z_2$) intersects with the two CBs within the ERs, which means that the phase difference of the two impedances crosses over $\pm 180^\circ$ within the ERs, there will be crossings over R on the Nyquist plot, as denoted by the red dots in Fig. 2.
3) *Step 3:* The crossing types can be determined by the derivatives of the impedance frequency responses. At each crossing frequency denoted by the red dot, if the phase derivative of the numerator impedance (Z_1) is less than that of the denominator impedance (Z_2), the crossing type will be a CC, and vice versa for an ACC.
4) *Step 4:* The total number of crossings can be calculated by the given formulas in Table II. For all $f \neq 0$, the crossing number should be doubled, whereas for $f = 0$, the crossing number should be counted separately. In most cases of the impedance-based stability analysis, the crossing number at 0 Hz is zero, since 0 Hz is out of the ER. However, if 0 Hz within ER occurs in some cases, how to determine the crossing number can be referred to [36]. Then the total number of crossings can be calculated by (9).

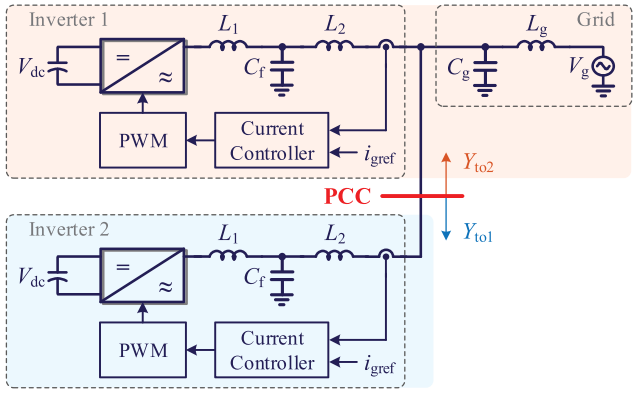

Fig. 3. Paralleled inverter system.

With the proposed method, the number of crossings can be directly obtained through the Bode plots of Z_1 and Z_2, and there is no need to calculate the minor-loop gain and draw the corresponding Nyquist plot. Among the four steps, Steps 1 and 2 follow the principle of the existing stability analysis methods, which only considers the magnitude and phase values of the frequency response. Yet, Steps 3 and 4 introduce new procedures, wherein the derivatives of the frequency response is involved in Step 3, and the response at 0 Hz is considered in Step 4.

D. Stability Prediction and Impedance Specification

Given the number of open-loop RHP poles and the number of encirclements, the system will be stable if and only if

$$\mathcal{N}_{\mathrm{CC}}[Z_1/Z_2] - \mathcal{N}_{\mathrm{ACC}}[Z_1/Z_2] = -\mathcal{P}[Z_1] - \mathcal{Z}[Z_2]. \quad (12)$$

It is worth mentioning that the stability prediction always follow the principle of the NSC, yet the analysis on Bode plots of individual impedances enables to specify the impedance profiles even when there are open-loop RHP poles. This is the unique contribution of the proposed method.

For an interconnected system, assuming one impedance (i.e., Z_1) unchanged, the other impedance (i.e., Z_2) can be specified and reshaped to cross over the CBs anticlockwise in the ERs the same times as the number of open-loop RHP poles in order to stabilize the whole system. This impedance shaping feature remarkably facilitates the design-oriented stability analysis for interconnected converter systems.

IV. CASE STUDIES AND EXPERIMENTAL VALIDATIONS

The stability analyses and experiments on a paralleled grid-tied inverter system are carried out in this section to validate the proposed method. The system configuration is displayed in Fig. 3. Two inverters are connected to the grid, and the grid-side current control is implemented with the proportional-resonant (PR) controller. All the parameters are listed in Table III. The equivalent series resistances (ESRs) of inductors are selected from the measured results in the experimental setups. The two inverters have the identical parameters.

TABLE III
SYSTEM PARAMETERS

Parameters	Values	Parameters	Values
V_{dc}	730 V	L_1	2 mH
V_{grms} (line to line)	400 V	L_2	1 mH
L_g	1 mH	ESRs of L_1 and L_2	0.4 Ω
ESR of L_g	0.4 Ω	C_f	10 μF
C_g	2 μF	K_p[a]	8 Ω
f_s[c]	10 kHz	K_r[b]	500 Ω/s

Notes: a and b. K_p and K_r—parameters of the current-loop PR controller.
c. f_s—sampling frequency, which is also equal to the switching frequency.

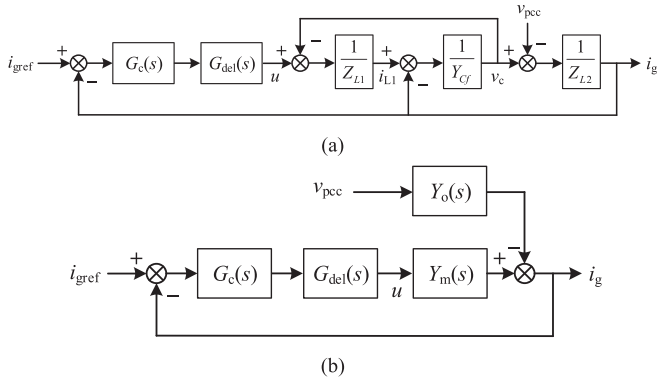

Fig. 4. Small-signal model of the inverter. (a) Comprehensive diagram. (b) Simplified diagram.

Since the two inverters have stable output admittances, and the grid impedance is passive with a stable output admittance, the system can be regarded as a $Y+Y$ system. In this case, the admittance ratio is adopted for analysis. To validate the proposed method, it is crucial to generate the RHP zeros in the admittance aggregation.

A. System Modeling

Since the admittance ratio is adopted for analysis, the inverter admittance and grid admittance are derived, respectively. The inverter admittance can be derived from the small-signal model provided in Fig. 4(a) [37].

In Fig. 4(b), the simplified admittances Y_o and Y_m can be derived from Fig. 4(a) as

$$Y_o(s) = \frac{Z_{L1}+Z_{Cf}}{Z_{Cf}Z_{L1}+Z_{L1}Z_{L2}+Z_{Cf}Z_{L2}} \tag{13}$$

$$Y_m(s) = \frac{Z_{Cf}}{Z_{Cf}Z_{L1}+Z_{L1}Z_{L2}+Z_{Cf}Z_{L2}}. \tag{14}$$

The PR controller is used for the current loop control whose transfer function is

$$G_c(s) = K_p + \frac{2K_r\omega_c s}{s^2+2\omega_c s+\omega_1^2} \tag{15}$$

where K_p and K_r are the P and R parameters, ω_1 is the fundamental angular frequency, and ω_c is selected as 3.14 rad/s to slightly widen the bandwidth of the PR controller [38].

G_{del} denotes the transfer function of the delay, which can be expressed by the Pade approximation [21]. In this article, a third-order Pade approximation is used, which leads to

$$G_{del}(s) = \text{Pade}\left(e^{-1.5T_s s}, 3\right) = \frac{1+\frac{1}{2}(-1.5T_s s)+\frac{1}{8}(-1.5T_s s)^2+\frac{1}{48}(-1.5T_s s)^3}{1-\frac{1}{2}(-1.5T_s s)+\frac{1}{8}(-1.5T_s s)^2-\frac{1}{48}(-1.5T_s s)^3}. \tag{16}$$

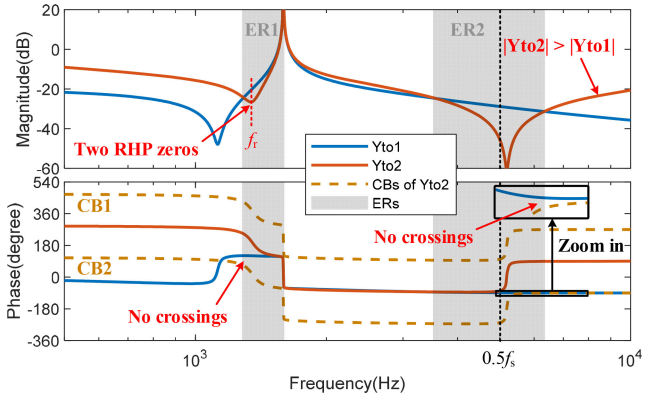

Fig. 5. Admittance Bode plots of Y_{to1} and Y_{to2}.

In the inverter model, the impacts of the phase-locked loop are neglected by selecting a sufficiently low control bandwidth for synchronizing with the grid. Thus the inverter model can be represented in the single-input single-output form [39]. The derived inverter output admittance is

$$Y_{io}(s) = \frac{Y_o(s)}{1+G_c(s)G_{del}(s)Y_m(s)}. \tag{17}$$

The grid admittance can be easily deduced as

$$Y_g(s) = sC_g + \frac{1}{sL_g}. \tag{18}$$

For the stability analysis, a PCC should be selected first, which divides the whole system into two subsystems. In the analysis of this article, the Inverter 1 and the grid are regarded as one subsystem, because this aggregation can introduce RHP zeros in the resultant admittance, i.e., Y_{to2}. The Inverter 2 is regarded as the other subsystem, whose admittance is denoted as Y_{to1}. Therefore, the PCC is selected as shown in Fig. 3.

B. Stability Analysis

Based on the PCC given in Fig. 3, Y_{to1} is the admittance of the Inverter 2, and Y_{to2} is the aggregated admittance of the Inverter 1 and the grid. The admittance Bode plots of Y_{to1} and Y_{to2} are plotted in Fig. 5. It can be seen that $|Y_{to2}| > |Y_{to1}|$ at high frequencies, thus it is better to use the admittance ratio Y_{to1}/Y_{to2} for stability analysis according to (3).

However, from the pole-zero map of Y_{to1} and Y_{to2} in Fig. 6, there is a pair of conjugate RHP zeros observed in Y_{to2}. Thus, there are two RHP poles produced in the admittance ratio Y_{to1}/Y_{to2}. For the conventional stability analysis methods, the Nyquist plot of Y_{to1}/Y_{to2} has to be checked due to the presence of open-loop RHP poles, as shown in Fig. 7. It can be found that the Nyquist trajectory does not encircle the critical point,

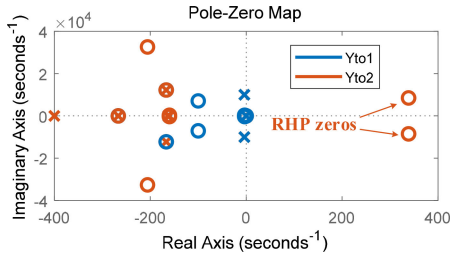

Fig. 6. Admittance pole-zero maps of $Y_{\rm to1}$ and $Y_{\rm to2}$.

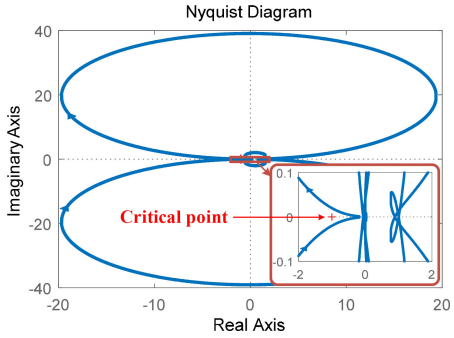

Fig. 7. Nyquist plot of the admittance ratio $Y_{\rm to1}/Y_{\rm to2}$.

which implies an unstable system. Although the Nyquist plot of the admittance ratio can predict the stability, it provides little insight into the impedance specifications.

With the proposed method, the system stability can be predicted directly from the admittance Bode plot, without calculating the admittance ratio. The RHP poles in $Y_{\rm to1}$ and the RHP zeros in $Y_{\rm to2}$ should be checked first. It can be seen from Fig. 5 that there is an antiresonance at f_r in the magnitude plot of $Y_{\rm to2}$, where the corresponding phase change is $-180°$. This fact implies a pair of conjugate RHP zeros at f_r, and hence there are two RHP poles present in the admittance ratio $Y_{\rm to1}/Y_{\rm to2}$, which agrees with the result in Fig. 6. It is noted that the Bode plots can identify RHP zeros accurately in this case, since both subsystems have stable admittances.

In Fig. 5, there are two ERs where $|Y_{\rm to1}| > |Y_{\rm to2}|$, as denoted in the shaded areas. The two CBs are drawn by shifting the phase curve $\angle Y_{\rm to2}$ of $\pm 180°$. Within the two ERs, there is no crossing between the CBs and the phase curve $\angle Y_{\rm to1}$, which indicates no encirclement around the critical point for the Nyquist trajectory of $Y_{\rm to1}/Y_{\rm to2}$. The analysis result is the same as that obtained from Fig. 7. Hence, the total number of anticlockwise encirclements is not equal to the number of open-loop RHP poles, and the system is unstable.

Besides the analysis given in Fig. 5, which is based on the explicit analytical models of the admittances in the continuous domain, the stability analysis based on the frequency-scan method is also provided in Fig. 8, which illustrates that the proposed approach also works well for "black-box" models. In Fig. 8, the admittance Bode plots are obtained by the frequency-scan method in the simulation. Since the switching frequency is 10 kHz, the admittance Bode plots are only checked

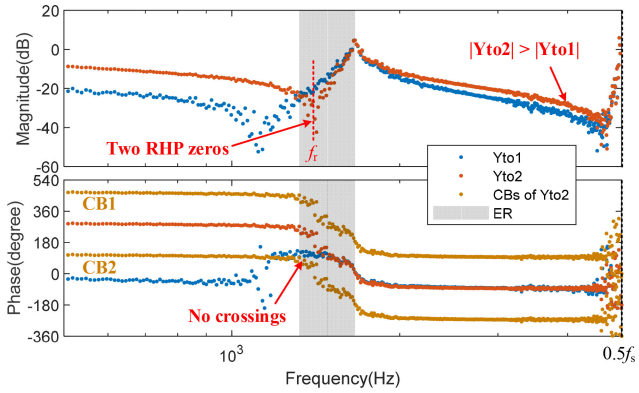

Fig. 8. Frequency-scanned admittance Bode plots of $Y_{\rm to1}$ and $Y_{\rm to2}$.

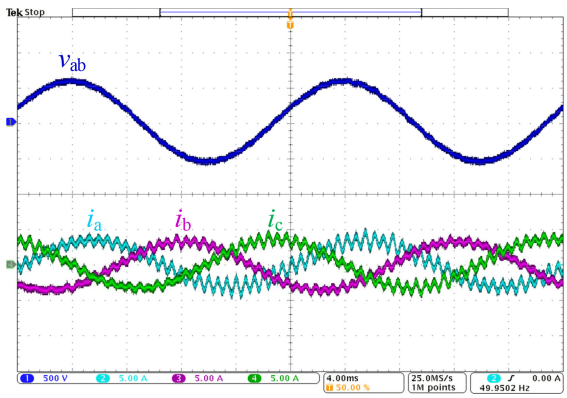

Fig. 9. Experimental waveforms of Case I.

until the Nyquist frequency, 5 kHz. It can be seen that the admittance plot is different from the continuous-domain model as shown in Fig. 5 around the Nyquist frequency, due to the impact of discretization. However, it is still true that $|Y_{\rm to2}| > |Y_{\rm to1}|$ at high frequencies, thus the admittance ratio $Y_{\rm to1}/Y_{\rm to2}$ can be utilized for stability analysis. Also, two RHP zeros can be found at the resonant frequency f_r in $Y_{\rm to2}$, and no crossing is found in the ER, then the system is, therefore, unstable.

The experimental waveforms for this case (Case I) are presented in Fig. 9. The waveform in CH1 is the line-to-line voltage at the PCC, and the waveforms in CH2–CH4 are the output currents for the Inverter 1. It can be seen that the system is unstable, which is predicted by the stability analysis.

Case I shows that the proposed method using Bode plots works well in the stability analysis of both "white-box" and "black-box" models. Especially for cases with the open-loop RHP poles, there is no need to check the zero-pole maps and draw the Nyquist plot of the impedance/admittance ratio.

C. Impedance Specification

In Case I the system is unstable, since there is no crossing within the ERs when the open-loop RHP poles exist. In this part, Case II is provided showing that the proposed method can implement impedance specifications to stabilize the system. In this case, $Y_{\rm to2}$ is unchanged to ensure the existence of the

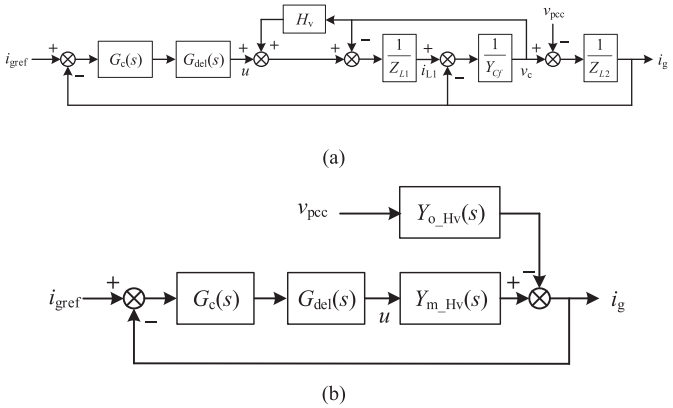

Fig. 10. Control diagram of the inverter considering the feedforward loop. (a) Comprehensive diagram. (b) Simplified diagram.

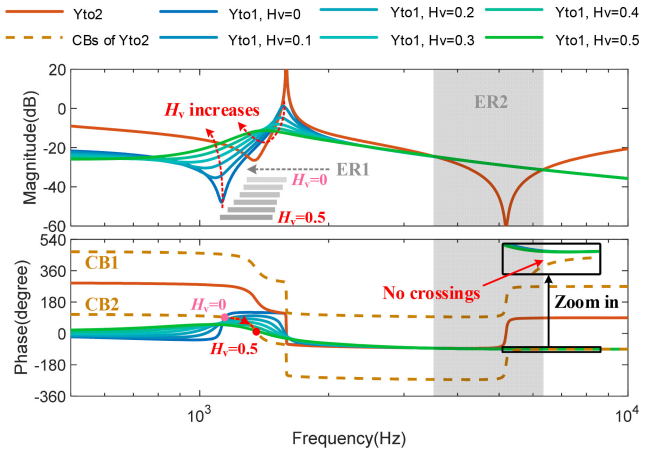

Fig. 11. Admittance specification by H_v.

open-loop RHP poles, and Y_{to1} is reshaped to guarantee the stability.

The way to stabilize the system is to specify the admittance Y_{to1} by letting $\angle Y_{\text{to1}}$ cross over the CB2 one times anticlockwise within the ERs (corresponding to two ACCs including the negative frequency range). Here the capacitor- voltage feedforward coefficient H_v is considered in the control loop, as shown in the control diagram in Fig. 10. Considering the feedforward loop, the equivalent admittances Y_{o_Hv}, Y_{m_Hv}, and the output admittance $Y_{\text{io\_Hv}}$ can be derived as

$$Y_{o\_Hv}(s) = \frac{Z_{L1} + Z_{Cf}(1 - H_v)}{Z_{L1}Z_{L2} + Z_{L1}Z_{Cf} + Z_{L2}Z_{Cf}(1 - H_v)} \tag{19}$$

$$Y_{m\_Hv}(s) = \frac{Z_{Cf}}{Z_{L1}Z_{L2} + Z_{L1}Z_{Cf} + Z_{L2}Z_{Cf}(1 - H_v)} \tag{20}$$

$$Y_{io\_Hv}(s) = \frac{Y_{o\_Hv}(s)}{1 + G_c(s)\,G_{\text{del}}(s)\,Y_{m\_Hv}(s)}. \tag{21}$$

With H_v selected from 0 to 0.5, the admittance Bode plots of Inverter 2, i.e., Y_{to1}, are plotted in Fig. 11. From the magnitude plot, the ER1 will move slightly to the lower frequency range,

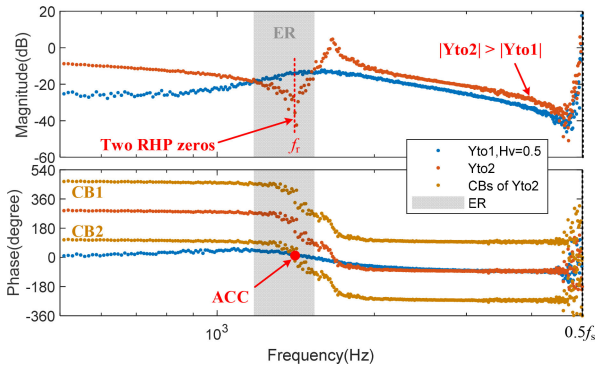

Fig. 12. Frequency-scanned admittance Bode plot for Case II.

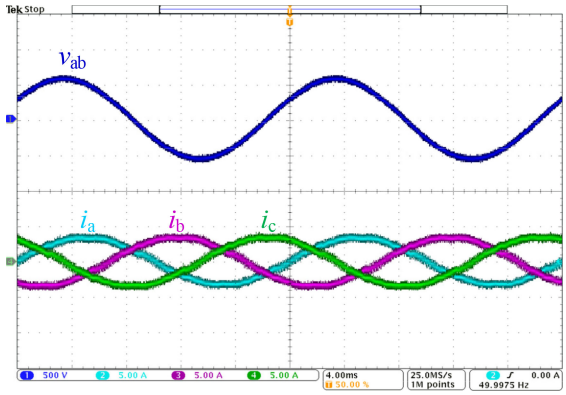

Fig. 13. Experimental waveforms for Case II.

as H_v increases. While on the phase plot, the pink dot denotes the original intersection point of $\angle Y_{\text{to1}}$ and CB2 when $H_v = 0$, which is outside the ER1. It can be seen that as H_v increases to 0.5, the intersection point will move to the red dot, which goes into the ER1 finally. If a closer look is taken at the crossing point, the derivative of $\angle Y_{\text{to1}}$ is larger than that of $\angle Y_{\text{to2}}$, therefore this is an ACC. Then including the negative-frequency range, the total number of ACCs should be two, which equals to the number of open-loop RHP poles, and the system can be stabilized.

Fig. 12 presents the frequency-scanned admittance Bode plots when $H_v = 0.5$ is adopted in Inverter 2 (Case II). It can be seen that within the ER, the phase plot of Y_{to1} has an ACC with CB2, thus the total number of ACCs is two including the negative frequency range, which equals to the total number of open-loop RHP poles, and the system is stable. Fig. 13 shows the experimental result with $H_v = 0.5$ for Inverter 2, indicating that the system is now stabilized.

Case II shows that with the proper design of H_v, the admittance Y_{to1} can be specified and reshaped to meet the stability condition, even when the open-loop RHP poles exist. Consequently, the proposed method can provide intuitive guidance for the converter controller designs.

V. Conclusion

This article has put forward a general impedance-based stability analysis method based on Bode plots of individual

impedances, which is applicable for analysis of interconnected converter systems with open-loop RHP poles present in the impedance ratio. The derivatives of the frequency response versus frequency, which was ignored in the conventional analysis, is considered in the proposed method. Two case studies in experiments have demonstrated the effectiveness and superior features of the proposed method, which are as follows.

1) The analysis based on the proper impedance ratio provides a more general approach, which does not rely on the subsystem types, and is able to address the cases with RHP poles present in the impedance ratio. Thus, it can be generalized to different types of interconnected converter systems and works for "black-box" models.
2) The method allows analyzing the system stability based on Bode plots of individual impedances, and no need to calculate the impedance ratio or the impedance sum, which enables to specify the impedance profile and implement the controller design-oriented analysis.

REFERENCES

[1] X. Wang and F. Blaabjerg, "Harmonic stability in power electronic based power systems: Concept, modeling, and analysis," *IEEE Trans. Smart Grid*, vol. 10, no. 3, pp. 2858–2870, May 2019.

[2] J. M. Undrill and T. E. Kostyniak, "Subsynchronous oscillations, part 1—Comprehensive system stability analysis," *IEEE Trans. Power App. Syst.*, vol. PAS–95, no. 4, pp. 1446–1455, Jul./Aug. 1976.

[3] R. D. Middlebrook, "Input filter considerations in design and application of switching regulators," in *Proc. IEEE Ind. Appl. Soc. Annu. Meeting*, 1976, pp. 91–107.

[4] C. M. Wildrick, F. C. Lee, B. H. Cho, and B. Choi, "A method of defining the load impedance specification for a stable distributed power system," *IEEE Trans. Power Electron.*, vol. 10, no. 3, pp. 280–285, May 1995.

[5] C. M. Wildrick, "Stability of distributed power supply systems," M.S. thesis, Virginia Power Electron. Center, Virginia Tech., Blacksburg, VA, USA, Feb. 1993.

[6] X. Feng, Z. Ye, K. Xing, F. C. Lee, and D. Borojevich, "Individual load impedance specification for a stable dc distributed power system," in *Proc. IEEE Appl. Power Electron. Conf.*, Dallas, TX, USA, Mar. 1999, pp. 923–929.

[7] X. Feng, J. Liu, and F. C. Lee, "Impedance specifications for stable DC distributed power systems," *IEEE Trans. Power Electron.*, vol. 17, no. 2, pp. 157–162, Mar. 2002.

[8] A. Li and D. Zhang, "Necessary and sufficient stability criterion and new forbidden region for load impedance specification," *Chin. J. Electron.*, vol. 23, no. 3, pp. 628–634, Jul. 2014.

[9] J. M. Zhang, X. G. Xie, D. Z. Jiao, and Z. M. Qian, "Stability problems and input impedance improvement for cascaded power electronic systems," in *Proc. IEEE Appl. Power Electron. Conf.*, Anaheim, CA, USA, 2004, pp. 1018–1024.

[10] B. Wen, D. Boroyevich, R. Burgos, P. Mattavelli, and Z. Shen, "D-Q impedance specification for balanced three-phase AC distributed power system," in *Proc. IEEE Appl. Power Electron. Conf.*, Charlotte, NC, USA, Mar. 2015, pp. 2757–2771.

[11] B. Wen, R. Burgos, D. Boroyevich, P. Mattavelli, and Z. Shen, "AC stability analysis and dq frame impedance specifications in power-electronics-based distributed power systems," *IEEE J. Emerg. Select. Top. Power Electron.*, vol. 5, no. 4, pp. 1455–1465, Dec. 2017.

[12] S. D. Sudhoff, S. F. Glover, P. T. Lamm, D. H. Schmucker, and D. E. Delisle, "Admittance space stability analysis of power electronic systems," *IEEE Trans. Aerosp. Electron. Syst.*, vol. 36, no. 3, pp. 965–973, Jul. 2000.

[13] S. D. Sudhoff and J. M Crider, "Advancements in generalized immittance based stability analysis of DC power electronics based distribution systems," in *Proc. IEEE Elect. Ship Tech. Symp.*, Alexandria, VA, USA, Apr. 2011, pp. 207–212.

[14] T. Suntio, J. Leppaaho, J. Huusari, and L. Nousiainen, "Issues on solar-generator interfacing with current-fed MPP-tracking converters," *IEEE Trans. Power Electron.*, vol. 25, no. 9, pp. 2409–2419, Sep. 2010.

[15] J. Sun, "Impedance-based stability criterion for grid-connected inverters," *IEEE Trans. Power Electron.*, vol. 26, no. 11, pp. 3075–3078, Nov. 2011.

[16] F. Liu, J. Liu, B. Zhang, H. Zhang, S. U. Hasan, and S. Zhou, "Unified stability criterion of bidirectional power flow cascade system," in *Proc. IEEE Appl. Power Electron. Conf.*, Long Beach, CA, USA, Mar. 2013, pp. 2618–2623.

[17] X. Zhang, X. Ruan, and C. K. Tse, "Impedance-based local stability criterion for dc distributed power systems," *IEEE Trans. Circuits Syst. I, Fundam. Theory Appl.*, vol. 62, no. 3, pp. 916–925, Mar. 2015.

[18] F. Liu, J. Liu, H. Zhang, and D. Xue, "Stability issues of Z + Z type cascade system in hybrid energy storage system (HESS)," *IEEE Trans. Power Electron.*, vol. 29, no. 11, pp. 5846–5859, Nov. 2014.

[19] F. Liu, J. Liu, H. Zhang, D. Xue, S. U. Hasan, and L. Zhou, "Stability issues of Z + Z or Y + Y type cascade system," in *Proc. IEEE Energy Convers. Congr. Expo.*, 2013, pp. 434–441.

[20] H. Liu, X. Xie, X. Gao, H. Liu, and Y. Li, "Stability analysis of SSR in multiple wind farms connected to series-compensated systems using impedance network model," *IEEE Trans. Power Syst.*, vol. 33, no. 3, pp. 3118–3128, May 2018.

[21] X. Wang, F. Blaabjerg, and P. C. Loh, "An impedance-based stability analysis method for paralleled voltage source converters," in *Proc. Int. Power Electron. Conf.*, 2014, pp. 1529–1535.

[22] I. Postlethwaite, "A generalized inverse Nyquist stability criterion," *Int. J. Control*, vol. 26, no. 3, pp. 325–340, 1977.

[23] B. Wen, D. Boroyevich, R. Burgos, P. Mattavelli, and Z. Shen, "Inverse Nyquist stability criterion for grid-tied inverters," *IEEE Trans. Power Electron.*, vol. 32, no. 2, pp. 1548–1556, Feb. 2017.

[24] B. J. Lurie and P. J. Enright, *Classical Feedback Control With MATLAB and Simulink*. Boca Raton, FL, USA: CRC Press, Taylor & Francis Group, 2011.

[25] H. Nyquist, "Regeneration theory," *Bell Syst. Tech. J.*, vol. 11, no. 1, pp. 126–147, Jan. 1932.

[26] B. Wen, D. Dong, D. Boroyevich, R. Burgos, P. Mattavelli, and Z. Shen, "Impedance-based analysis of grid-synchronization stability for three-phase paralleled converters," *IEEE Trans. Power Electron.*, vol. 31, no. 1, pp. 26–38, Jan. 2016.

[27] G. F. Franklin, J. D. Powell, and A. Emami-Naeini, *Feedback Control of Dynamic Systems*. London, U.K.: Pearson Educ., 2015.

[28] R. Pintelon, P. Guillaume, Y. Rolain, J. Schoukens, and H. V. Hamme, "Parametric identification of transfer functions in the frequency domain—A survey," *IEEE Trans. Automat. Control*, vol. 39, no. 11, pp. 2245–2260, Nov. 1994.

[29] H. Liu, X. Xie, and W. Liu, "An oscillatory stability criterion based on the unified DQ-frame impedance network model for power systems with high-penetration renewables," *IEEE Trans. Power Syst.*, vol. 33, no. 3, pp. 3472–3485, May 2018.

[30] H. Bode, *Network Analysis and Feedback Amplifier Design*, New York, NY, USA: D. Van Nostrand Company, 1945, pp. 157–162.

[31] Y. Liao and X. Wang, "General rules of using Bode plots for impedance-based stability analysis," in *Proc. IEEE Workshop Control Model. Power Electron.*, Padova, Italy, 2018, pp. 1–6.

[32] J. Hahn, T. Edison, and T. F. Edgar, "A note on stability analysis using Bode plots," *Chem. Eng. Educ.*, vol. 35, no. 3, pp. 208–211, 2001.

[33] M. Vidyasagar, D. G. Meyer, and G. F. Franklin, "Some simplifications of the graphical Nyquist criterion," *IEEE Trans. Automat. Control*, vol. 33, no. 3, pp. 301–305, 1988.

[34] F. Stratulat and F. Ionescu, *Linear Control Systems—Analysis and Synthesis, Theory and Applications*. Stuttgart, Germany: Stenbeis-Edition, 2009.

[35] D. Lumbreras, E. L. Barrios, A. Ursúa, L. Marroyo, and P. Sanchis, "On the stability criteria for inverter current control loops with LCL output filters and varying grid impedance," in *Proc. Euro. Conf. Power Electron. Appl.*, 2017, pp. 1–10.

[36] D. Lumbreras, E. L. Barrios, A. Urtasun, A. Ursúa, L. Marroyo, and P. Sanchis, "On the stability of advanced power electronic converters: The generalized Bode criterion," *IEEE Trans. Power Electron.*, vol. 34, no. 9, pp. 9247–9262, Sep. 2019.

[37] X. Wang, F. Blaabjerg, M. Liserre, Z. Chen, J. He, and Y. Li, "An active damper for stabilizing power-electronics-based AC systems," *IEEE Trans. Power Electron.*, vol. 29, no. 7, pp. 3318–3329, Nov. 2014.

[38] R. Teodorescu, F. Blaabjerg, M. Liserre, and P. C. Loh, "Proportional-resonant controllers and filters for grid-connected voltage-source converters," *IEE Proc. Elec. Power Appl.*, vol. 153, no. 5, pp. 750–762, Sep. 2006.

[39] X. Wang, F. Blaabjerg, and W. Wu, "Modeling and analysis of harmonic stability in an AC power-electronics-based power system," *IEEE Trans. Power Electron.*, vol. 29, no. 12, pp. 6421–6432, Dec. 2014.

Yicheng Liao (S'16) received the B.S. degree in electrical engineering and its automation and the M.S. degree in electrical engineering from Southwest Jiaotong University, Chengdu, China, in 2015 and 2018, respectively. She is currently working toward the Ph.D. degree in power electronic engineering with Aalborg University, Aalborg, Denmark.

In July 2017, she was a Visiting Student with Ecole Polytechnique and Inria, Paris, France. Since January 2018, she has been with the Department of Energy Technology, Aalborg University. Her research interests include the modeling and stability analysis of power electronics-based power systems.

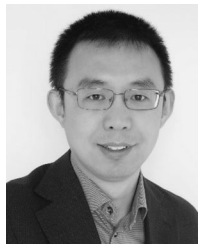

Xiongfei Wang (S'10–M'13–SM'17) received the B.S. degree in electrical engineering from Yanshan University, Qinhuangdao, China, in 2006, the M.S. degree in electrical engineering from Harbin Institute of Technology, Harbin, China, in 2008, and the Ph.D. degree in energy technology from Aalborg University, Aalborg, Denmark, in 2013.

Since 2009, he has been with the Department of Energy Technology, Aalborg University, where he became the Assistant Professor in 2014, Associate Professor in 2016, and Professor and Research Program Leader for Electronic Power Grid (eGrid) in 2018. His research interests include modeling and control of grid-interactive power converters, stability and power quality of power electronic based power systems, and active and passive filters.

Dr. Wang was selected into Aalborg University Strategic Talent Management Program in 2016. He was the recipient of the six IEEE Prize Paper Awards, the 2017 Outstanding Reviewer Award of IEEE TRANSACTIONS ON POWER ELECTRONICS, the 2018 IEEE PELS Richard M. Bass Outstanding Young Power Electronics Engineer Award, and the 2019 IEEE PELS Sustainable Energy Systems Technical Achievement Award. He serves as an Associate Editor for the IEEE TRANSACTIONS ON POWER ELECTRONICS, IEEE TRANSACTIONS ON INDUSTRY APPLICATIONS, and IEEE JOURNAL OF EMERGING AND SELECTED TOPICS IN POWER ELECTRONICS.